Experimental and numerical multi-scale approach for Sheet-Molding-Compound composites fatigue prediction based on fiber-matrix interface cyclic damage

S. Tamboura[a,*], H. Ayari[a,b], M. Shirinbayan[b], M.A. Laribi[b,c], H. Bendaly[a], H. Sidhom[d], A. Tcharkhtchi[b], J. Fitoussi[b]

[a] University of Sousse, Ecole Nationale d'Ingénieurs de Sousse, LMS, Pôle technologique, 4054 Sousse, Tunisia
[b] Arts et Métiers ParisTech, PIMM – UMR CNRS 8006, 151 Boulevard de l'Hôpital, 75013 Paris, France
[c] Institut Clément Ader, UMR CNRS 5312, University of Toulouse, Toulouse, France
[d] University of Tunis, ENSIT- Ecole Nationale Supérieure d'Ingénieurs de Tunis, LMMP, Av. Taha Hussein 1008, Tunisia

Keywords:
SMC
Fatigue
Young's modulus evolutions
Model
Fiber-matrix interface debonding

A B S T R A C T

In this paper, a multi-scale approach is proposed to predict the stiffness reduction of a Sheet-Molding-Compound (SMC) composite submitted to low cycle fatigue (until 2.10^5 cycles). Strain-controlled tensile fatigue tests ($R = 0.1$) are carried out at various strain ranges. Damage is investigated at both macroscopic and microscopic scales through the evolutions of Young's modulus and SEM observations, after interrupted fatigue tests at different lifetime periods. The results show that the fatigue degradation of the composite is mainly controlled by fiber-matrix interface debonding. A quantitative analysis allows determining the threshold and kinetics of the fiber-matrix interface damage during cyclic loading as a function of the orientation of fibers. Moreover, a fiber-matrix interface damage criterion, taking into account the local cyclic normal and shear stresses at the interface, is introduced in the Mori and Tanaka approach in order to predict the loss of stiffness. The parameters of this local criterion are identified by reverse engineering on the basis of the experimental results described above. Finally, the predicted loss of stiffness is very consistent with the experimental results.

1. Introduction

Composite materials are becoming increasingly attractive because of their ease of fabrication, relatively low cost, low density and good mechanical properties compared to their weight [1–6]. To design discontinuous fiber composite structures, it is imperative to predict their behavior as a function of microstructure and damage. Indeed, as damage affects the performance of polymers and the structures of composites, the comprehensive description, detection and prediction of local damage mechanismsare scientifically and industrially important and valuable [7]. However, local damage mechanisms occurring in discontinuous fiber reinforced composites at the local scale are multiple and complex and need substantial experimental investigation to be described properly. Different damage modes can be activated simultaneously, involving complex coupling. Thus, the prediction of the threshold and kinetics of damage becomes a difficult task.

Moreover, the most critical degradation of discontinuous fiber reinforced composite structures has been observed for fatigue and impact loading [7]. Applying cyclic loading generally results in progressive damage accumulation related to the degradation of macroscopic mechanical properties such as stiffness reduction [8,9]. Fatigue damage can be described by nucleation, propagation, coalescence or/and stable growth of cracks, which leads to the final failure of the material [10].

For continuous fiber reinforced composites such as laminates, fatigue damage should be described by the progressive accumulation of transverse fatigue cracks observed at the transverse fiber interfaces [11]. In that case, final failure occurs when delamination between two adjacent plies takes place together with fiber breakage in different orientations [10]. For unidirectional composite fatigue, two dominant stages involving an initially high but decreasing damage rate followed by a slowly increasing rate have been observed [12].

On the other hand, for discontinuous fiber reinforced polymers, a lot

of studies have revealed that the fiber-matrix interface failure can be defined as the predominant local damage mechanism [13–22]. The experimental analysis has revealed that local damage generally begins by debonding the most misoriented fibers when the local normal stress reaches a critical value. Then, it progressively propagates to less misoriented fibers by coupling normal and shear interface stresses [15]. Under tension, damage initiation is generally observed for 20% to 30% of the failure stress [14–22]. For short fiber reinforced thermoplastic, the ductility of the matrix around the fibers leads to diffuse microcracking. Some researchers talked about a damaged interphase zone [5,7]. In this study, the fatigue damage of Sheet Molding Compounds (SMCs) is investigated. SMCs present a high strength-to-weight ratio and a high capacity of energy absorption during impact [14–22]. They are composed of glass fibers, unsaturated polyester, phenolic, vinyl, acrylic or modified resins to generally produce a strong molding compound [14–22]. We present in this paper microscopic-macroscopic relationships, while considering damage, and we propose a predictive approach of fatigue stiffness reduction.

First, an experimental multiscale analysis of damage under tension cyclic loading is presented. A quantitative analysis allows emphasizing the threshold and kinetics of fiber-matrix interface debonding as a function of the fiber orientation. Second, the experimental results are used to identify a fatigue micromechanical model in order to predict the macroscopic stiffness reduction of a discontinuous randomly oriented fiber reinforced polyester, noted hereafter as SMC R42.

Local damage is introduced in a Mori and Tanaka approach through a probabilistic Weibull's form an interface failure criterion to consider the statistical aspects of local failure. Moreover, the cyclic loading effect is introduced by a progressive modification of the fiber-interface strength related to local cyclic loading. The experimental quantitative local analysis is then used to identify the evolution of the interfacial strength during fatigue by reverse engineering. Therefore, the suggested model is an extension of the Jendli [23] model, originally developed for monotonic loading to cyclic damage.

The main objective of this work is to describe the fatigue stiffness reduction of SMC composites. The experimental and numerical work presented here is limited to low cycle fatigue: between 10^3 to 2.10^5 cycles to failure. In Section 2, the material characteristics and experimental procedures are presented. Section 3 is devoted to the description of the damage micromechanical model. The general approach and the main constitutive equations are also described. In Section 4 the algorithm and numerical implementation of the fatigue local criterion are shown. The identification and main equations are described in Section 5. Finally, a comparison between the experimental results and the numerical simulation are presented and discussed.

2. Materials and experimental methods

An SMC composite consists of an unsaturated polyester resin reinforced with glass fibers and is highly filled with calcium carbonate fillers ($CaCO_3$). The weight content of glass fibers is of 42%. Such fibers are presented in the form of bundles, and each bundle contains about 200 fibers. These fibers have a length of 25 mm with a diameter of about 15 μm.

2.1. Microstructure analysis

SMC plates are provided by the Plastic Omnium company auto exterior services from which samples are cut following the dimensions shown in Fig. 1.

Scanning Electron Microscopy (SEM) is performed to reveal the microstructure of SMCs (Fig. 2). This micrograph highlights a randomly oriented distribution of bundles of fibers where the ellipticity of the fibers is directly related to their orientation. The presence of CaCO3 particles and porosity in the matrix is also noticeable.

A quantitative study of the fiber orientation distribution is

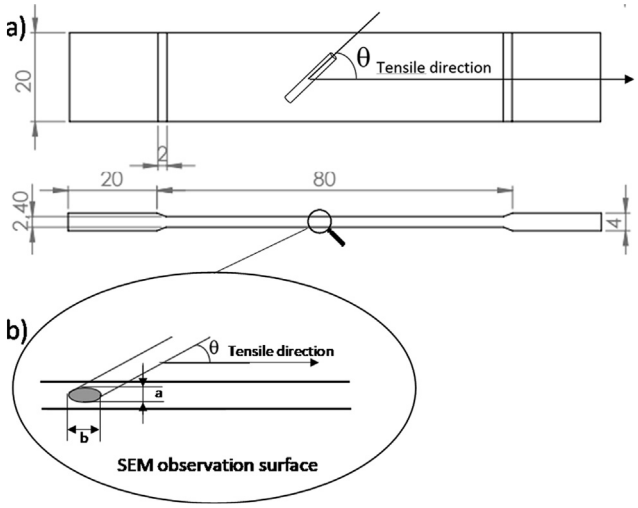

Fig. 1. (a) Specimen dimensions for tensile and fatigue tests, (b) Elliptic form of fiber appearing at surface.

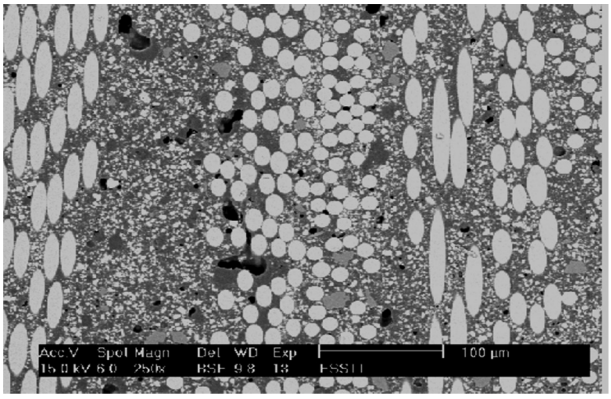

Fig. 2. Microstructure of SMC composite: Bundle of fibers.

performed by the SEM image analysis through the determination of the ellipticity of the fibers appearing on the polished surface. The following simple geometric relation allows determining the in-plane orientation of a fiber inside a bundle: θ = arc sin (a/b), where "a" and "b" are respectively the short and long axes of the ellipse. Once the orientation of a fiber family (θ) is determined, the quantification of the fiber volume fraction of this family, f(θ), is given by Eq. (1) [16]:

$$f(\theta) = \frac{n_\theta . n_B . s}{S} = \frac{n_\theta . f_m(\theta) . s(\theta)}{S} \quad (1)$$

where n_θ is the number of bundles oriented at θ, n_B is the number of fibers in a bundle, s is the surface of an ellipse of θ, S is the total surface, $f_m(\theta)$ is the volume fraction of fibers in the bundle oriented at θ, and $s(\theta)$ is the surface of a bundle (widely described and calculated in [16]). Fig. 3 shows the obtained distribution of the orientation of the SMC in study. The orientation of the fibers is predominant due to material flow during thermocompression.

2.2. Mechanical behavior and damage analysis methodology

Monotonic and cyclic tensile tests are performed on samples described in Fig. 1. Longitudinal and transverse strain gages are placed on the specimen surface. Maximum care was taken during the collage of the gages and false tests were not retained. Tensile tests are performed at a constant displacement rate of 5 mm/min. Tensile fatigue tests are conducted for three imposed maximum strains:

$\varepsilon = 0.50\%$; $\varepsilon = 0.64\%$; $\varepsilon = 0.8\%$ with a loading rate of R = 0.1 and

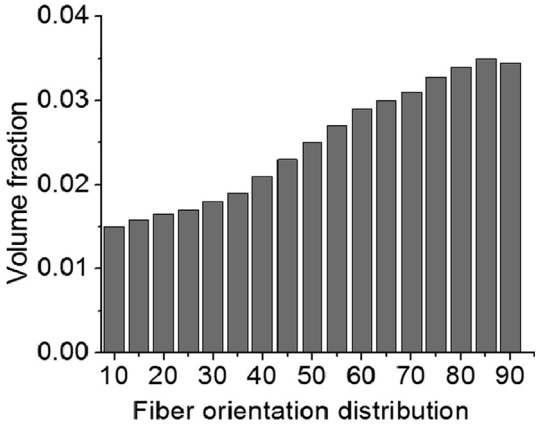

Fig. 3. Fiber orientation distribution in matrix of SMC R42 composite.

a frequency of 5 Hz. Three specimens are tested for each condition. The Young's modulus is measured during cyclic loading in order to determine the progressive loss of stiffness though the evolution of the relative Young's modulus: $\frac{E}{E_1}$ where E is the Young's modulus during cyclic loading and E_1 is the original Young's modulus measured at the first cycle.

Moreover, interrupted fatigue tests are performed in order to characterize the evolution of the damage mechanisms occurring at the local scale during cyclic loading. A representative observation area was previously marked on the SEM observation surface and analyzed qualitatively and quantitatively after each interruption. The observation area is chosen to be large enough (5×2.4 mm^2) to be statistically representative of the average microstructure in terms of fiber content and distribution of orientation (shown in Fig. 3).

In the next sections, we present a qualitative and quantitative analysis of the local damage due to cyclic loading. Finally, the macroscopic loss of stiffness is related to the local damage state evolution.

2.3. Qualitative analysis of local damage mechanisms during fatigue loading

The fatigue damage of composite materials generally goes through two stages: initiation and propagation. SEM micrographic investigations are carried out on the marked area, as described above, for all imposed deformations, and crack initiation at the fiber/matrix interfaces (Fig. 3) appears. Fiber-matrix interfaces present relatively low mechanical strength and are consequently transformed into preferential sites for micro-cracking. Under tension loading, such microcracks are generally perpendicular to the loading direction. Besides, this mechanism is known as predominant in SMC composites [14–23]. As in monotonic loading, fiber-matrix interface debonding always begins at the most disoriented fibers versus loading direction (Fig. 4a), and it progressively develops in all directions of reinforcement (Fig. 4b).

After the stage of initiation described above, interfacial microcracks coming from adjacent fibers merge into one larger microcrack (Fig. 5a). At this stage, each bundle may contain several perpendicular crossing microcracks (Fig. 5b). Then, decohesion spreads through the matrix, always in a direction almost perpendicular to the tensile direction, in order to join other microcracks coming from other fiber-matrix interface debonding (Fig. 5c). Coalescence leads to relatively long cracks compared to the fiber diameter. Finally, as observed by Shirinbayan et al. [21] for monotonic loading, the coalescence of these large microcracks leads to the final failure by the pseudo-delamination between bundles (Fig. 5d).

2.4. Quantitative analysis of local damage mechanisms during fatigue loading

Quantitatively relating the evolution of the crack densities at the local scale to the residual macroscopic properties of the composite during cyclic loading is of particular interest to build an accurate micromechanical model. This is the aim of this section.

As the fiber-matrix interface appears to be a weak point of the composite, special attention has been paid to fiber-matrix interface debonding. In need of simplification, the number of orientation families represented in Fig. 3 is reduced to six: 10°, 30°, 45°, 60°, 80°and 90°. Each bundle of fibers within the observation area is mapped and assigned to one of these six orientation families. Since every bundle was originally cut from the same roving, each bundle contains the same number of fibers, that is $n_B = 200$. After each fatigue test interruption, SEM observations are performed in order to determine the number of debonded fibers inside each bundle. Therefore, it is possible to define a local interface damage indicator for each fiber family of orientation during fatigue as: $d_\theta(N) = \frac{n_d^\theta}{n_B * n_\theta}$

where $n_d^\theta$is the total number of fibers presenting a broken interface contained inside the total number of bundles presenting the considered orientation θ (being n_θ), and N is the number of applied cycles. The evolutions of this interfacial damage indicator as a function of the number of cycles, for three values of the maximal imposed deformations ($\varepsilon = 0.50\%$; $\varepsilon = 0.64\%$; $\varepsilon = 0.8\%$), are reported in Fig. 6.

Independently of the imposed fatigue strain, the obtained results quantitatively confirm that the largest and fastest local damage is associated to the most disoriented fibers versus the loading axis ($\theta = 90°$). Indeed, independently of the imposed maximum strain, nearly 80% of the fibers oriented perpendicularly to the loading axis are submitted to debonding. Slightly disoriented fibers ($\theta = 10$–$15°$) contribute to damage only after an incubation period varying between 10^4 and 10^5

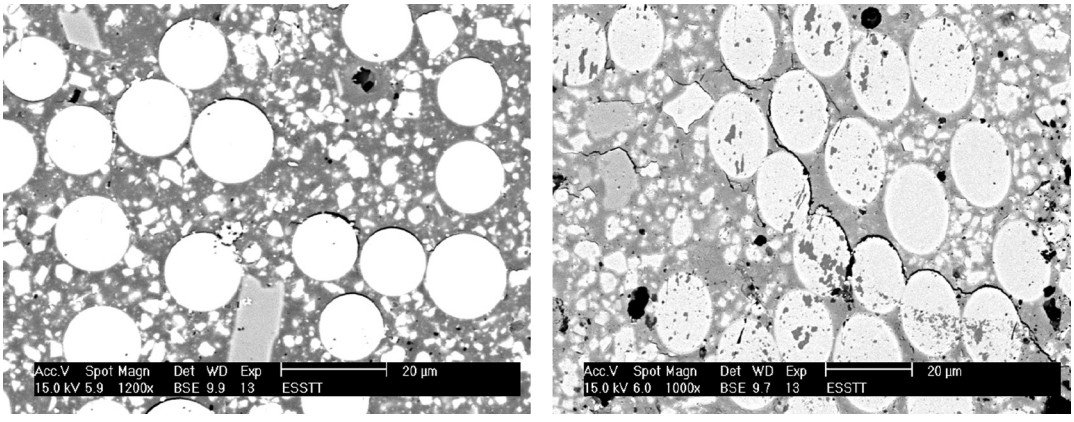

Fig. 4. Decohesion at fiber/matrix interfaces; (a) 90° oriented fibers (b) 45° oriented fibers.

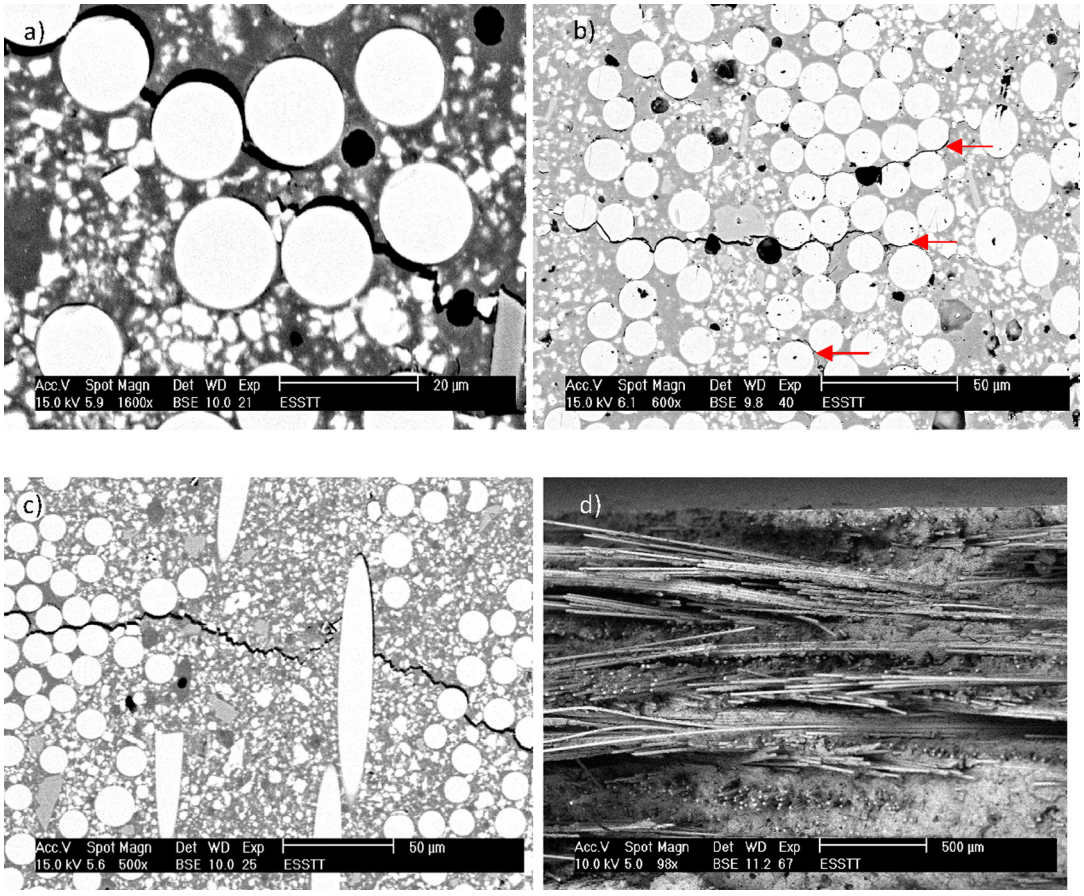

Fig. 5. Microcracks spreading under cyclic loading; (a) from one fiber to its neighbors; (b) multi-cracking of bundles; (b) and (c) from one bundle to its neighbors; (d) final failure by pseudo-delamination between bundles.

cycles and depending on the imposed maximum strain (Fig. 6). A great influence of the loading condition on the threshold and kinetics of damage can be noted. Indeed, the increase in fiber-matrix interface damage is more severe when the imposed maximum deformation is greater.

As already noted, to simplify the experimental work, only six families of the fiber orientation are analyzed. However, for micromechanical modeling purposes, it is important to get a precise description of the crack density evolutions for other intermediate orientations. For this, we can describe the evolution of the interfacial crack densities according to the number of cycles by the following form:

$$d_\theta^N = A_\theta ln(N) - B_\theta \tag{2}$$

where A_θ and B_θ are material parameters identified by fitting the curves of Fig. 5 for each θ orientation, and N indicates the number of cycles. Therefore, threshold values can be derived by:

$N_{th}^\theta = exp\left(\frac{B_\theta}{A_\theta}\right)$. In Section 4.2, the identified values of A_θ and B_θ for $\theta = 90^\circ$and $\theta = 45^\circ$will be used for the identification of the local cyclic fiber-matrix interface failure criterion.

3. Micromechanical modeling

The selection of a suitable model is mainly linked to the composite architecture. Thus, it is essential to consider the volume fractions of reinforcements, their size and the material symmetries. All the presented models adopt the Eshelby's equivalent inclusion method, except for the Voigt and Reuss bounds. Therefore, the reinforcement of ellipsoidal geometry is analytically taken into account. This geometry is characterized by the ratio l/d, where l and d are respectively the length and diameter of reinforcement. Accordingly, we can distinguish several forms: Long fibers if (l/d) tends to infinity.

- Short fibers if $10 < (l/d) < 50$.
- Particle if $1 < (l/d) < 5$.
- Disk if (l/d) tends to 0.

To choose the model that will give the best estimate of effective properties, the morphology of the material must be considered. For example, the least descriptive approach is that of Voigt or Reuss. Their simplicity is due to the fact that it takes into account only very few microstructural parameters. Indeed, it is only used when access to microstructural information is restricted. For instance, spatial distribution, orientation of reinforcement and its shapes are not opted for in this type of model. Only the elasticity tensors and volume ratios of each phase are used. Furthermore, the Hashin and Shtrikman model is limited to a few forms of reinforcement (long fibers, small disks, spherical reinforcement). In addition, bounded models, Voigt and Reuss or those of Hashin and Shtrikman, only provide a framework for the effective characteristics. Homogenization in a dilute solution is restricted to low volume ratios of reinforcement, which does not allow the consideration of different reinforcement interactions [24].

Among the different estimates, the self-consistent and Mori and Tanaka approaches have a larger scope given their ability to estimate the properties of materials with relatively big reinforcement ratios.

The material of our study has a volume fraction lower than 30%. This points us to the Mori and Tanaka model which is more suitable for such a reinforcement rate. Moreover, this model has the advantage of separately seeing a continuous matrix phase in which reinforcement is directly embedded, unlike the self-consistent approach which does not distinguish the phases in-between.

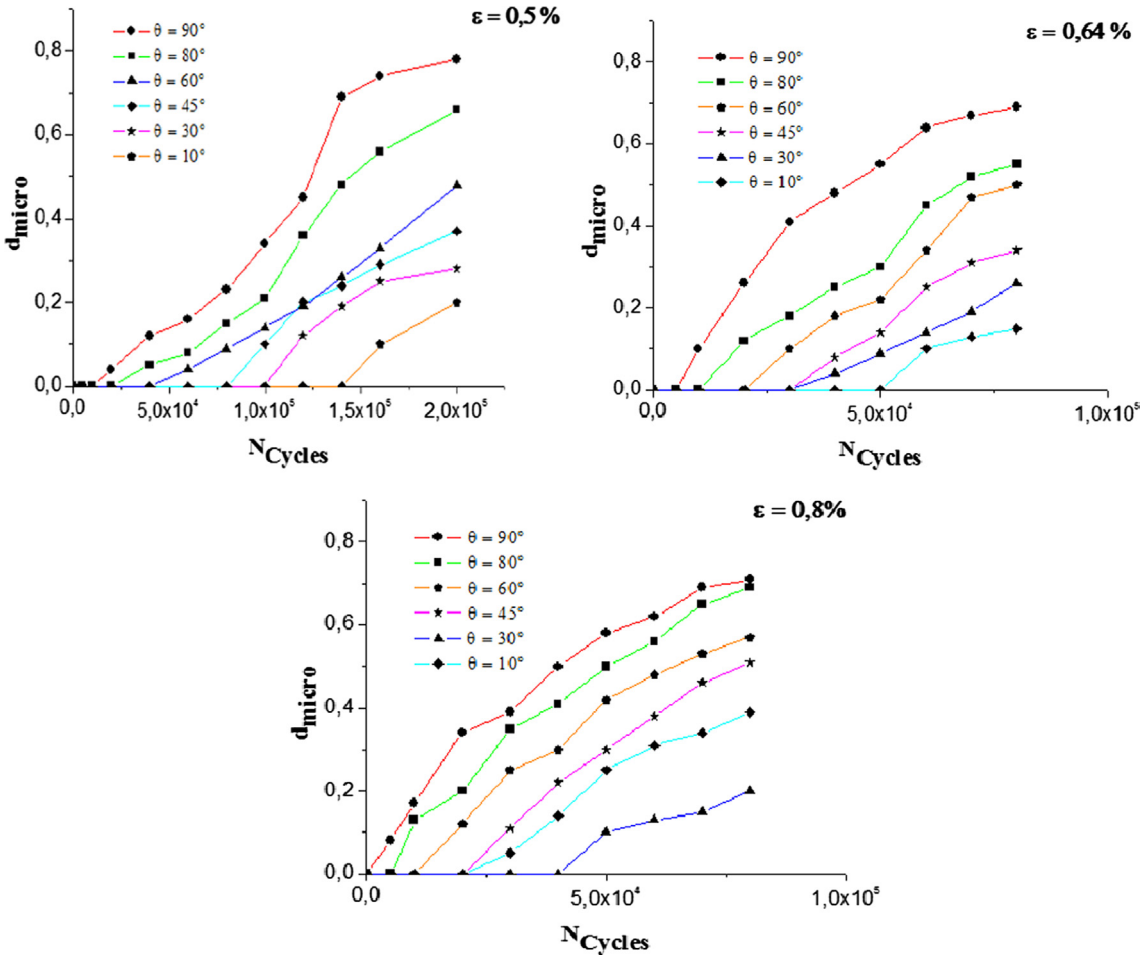

Fig. 6. Evolution of interfacial micro-cracking during fatigue tests for different fiber orientations and applied macroscopic strains; $\varepsilon = 0.50\%$, $\varepsilon = 0.64\%$, $\varepsilon = 0.8\%$.

Besides, this model has the advantage of analytical resolution, unlike the self-consistent model. In view of these elements, we consider that the Mori and Tanaka model is the most appropriate and will be retained for the rest of this study.

3.1. Basic equations

The micromechanical multi-scale modeling is based on the Mori and Tanaka approach [15]. Several authors, such as Fitoussi et al. [18,25,26], and Jendli et al. [23], have proposed to introduce damage into this approach through the identification of local damage criteria. Indeed, basic equations allow computing composite stiffness and average stress fields in different phases. Fiber-matrix interface stresses can be easily derived, as detailed hereafter. The matrix and the fibers are considered isotropic.

The composite stiffness tensor is given by the following expression:

$$C^{Comp} = C^m[I + f\langle \mathrm{Q}\rangle(I + f\langle (S - I)\mathrm{Q}\rangle)^{-1}]^{-1} \tag{3}$$

where $\langle \mathrm{Q}\rangle$ denotes the average, $\mathrm{C^m}$ and S are respectively the stiffness tensor of the matrix and the Eshelby tensor [17], and Q is a pseudo-localization tensor defined for each family of fiber orientation "θ" as:

$$\mathrm{Q}^\theta = ((C^m - C^\theta)(S^\theta - I) - C^\theta)^{-1}(C^\theta - C^m) \tag{4}$$

where C^θ represents the stiffness tensors of the reinforcement oriented at θ° (see Fig. 7). Note that for SMC composites, we can consider that all the fibers are contained in the plane of the plate. Therefore, each family of reinforcement is characterized only by its orientation in plane θ.

The aforementioned theory leads also to the expression of the local stress tensor in reinforcement as follows

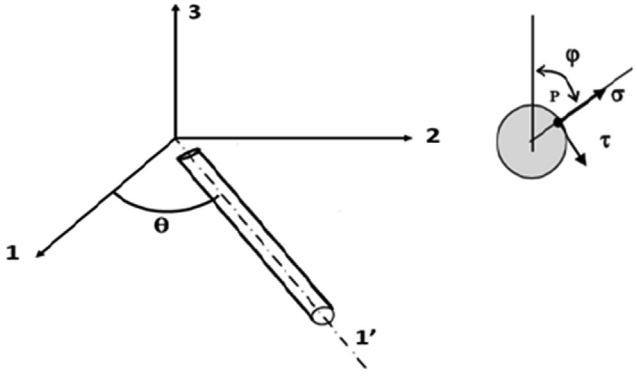

Fig. 7. Definition of normal and shear interface stresses, σ_n and τ, respectively.

$$\sigma^\theta = C^m(I + (S^\theta - I)\mathrm{Q}^\theta)(I + f\langle (S - I)\mathrm{Q}\rangle)\varepsilon^{imp} \tag{5}$$

Using the continuity condition of the normal stress at the interface, the average stress in the "θ" fiber family is used to compute the normal and shear interfacial stresses, σ_n and τ respectively, at each point located at the fiber-matrix interface (defined by φ,see Fig. 7).

Note that the interfacial stresses, σ_n and τ, can be computed on each interfacial point defined by angle φ, as illustrated in Fig. 10.

3.2. Local damage modeling

Therefore, we can define an interfacial failure probability computable at each fiber-matrix interface point defined by the fiber

orientations θ and φ (see Fig. 7):

$$P_r(\theta, \varphi) = 1 - exp\left(-\left(\left(\frac{\sigma}{\sigma_0}\right)^2 + \left(\frac{\tau}{\tau_0}\right)^2\right)^m\right) \quad (6)$$

where m is a statistical parameter related to the microstructure scatter. Normal and shear stresses σ_n and τ depend on the macroscopic applied stress, aspect ratio, volume fraction and orientation of the considered fibers and the elastic properties of the matrix and the fibers.

A given damaged state can be defined as a microstructure containing:

(1) Active fibers (noted f_n^{act}) contributing to the composite reinforcement and including two populations: the undamaged fibers (noted f_n^{nd}) and a part of the damaged ones, which partially help in composite reinforcement. Their contribution is defined by a reduction coefficient, "k", applied to the amount of debonded fibers
(2) Micro-cracks to be introduced (noted f_n^{mc}).

Hence, at each calculation step, n, the determination of the local interface failure probabilities (Eq. (9)) allows the description of the local damage state by the following equations:

$$f_n^{nd} = (1 - P_r^n) * f_{n-1}^{nd} \quad (7)$$

$$f_n^{act} = f_n^{nd} + k \sum_{i=1}^{n} P_r^i . f_{i-1}^{nd} \quad (8)$$

$$f_n^{mc} = f_{n-1}^{mc} + h . P_r^n . f_{n-1}^{nd} \quad (9)$$

Note that the reduction parameter "k" has been evaluated by finite element calculations performed on a representative cell containing a partially debonded fiber and which is equal to 0.5. Actually, "h" is the ratio between the volume of the introduced zero stiffness penny shape (representing an interfacial micro-crack) and the fiber volume evaluated by geometric considerations.

3.3. Monotonic tensile loading simulation

A tensile test is performed and simulated using this formalism. The orientation distribution determined in Section 2.1 issued as input data. At each increment of deformation, the interface failure probability is computed for each fiber orientation family, and the three heterogeneity populations described above are evaluated in order to determine the corresponding damage state as well as associated macroscopic stiffness and stresses. Finally, stress-strain curves and relative stiffness losses are plotted. Fig. 8 presents a comparison between the experimental and simulated results. For more details, [17,23] can be consulted.

Mostly, this simulation allowed the identification, by inverse engineering, of the fiber-matrix interface strength defined by σ_0 and τ_0. Indeed, for monotonic loading simulation, contrary to fatigue modeling (next paragraph), interface strength values σ_0 and τ_0 remain constant during loading. Therefore, these values should be considered as the initial ones in fatigue simulation, as described in the next section.

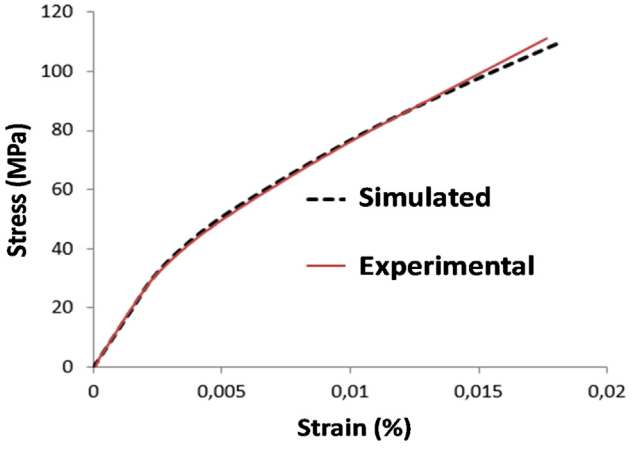

Fig. 8. Experimental and simulated stress-strain curves for SMC composite.

4. Micromechanical fiber-matrix interface cyclic damage modeling

4.1. Main idea

The experimental results obtained on SMC composites under fatigue loading show that a repeated applied stress leads to progressive diffuse damage of fiber-matrix interfaces. Indeed, at a local scale, the interface (or interphase) zone is submitted to local cyclic loading. Every interface location is submitted to a specific cyclic variation in local normal and shear stresses (σ,τ). The local amplitude can be evaluated by Eqs. (5)–(8). Thus, the local cyclic interfacial loading depends, among other factors, on the microstructure, the imposed macroscopic loading and the local orientation of the considered fiber.

As a consequence, we can consider that the local interface-interphase stresses (σ,τ) undergone cyclically by the interface zone may modify the limit stresses (σ_0, τ_0) as a result of two local phenomena:

(a) The local strain hardening of the polymer zone located on and just around the fiber (including sizing)
(b) The redistribution of the local stresses due to the diffused damage on the other interfacial sites

The first phenomenon is well known for glassy polymers, but it may also be observed for thermosets under several conditions such as confined cyclic loading and local self-heating [19,20]. It is generally associated to the reinforcement of the mechanical response resulting from large deformation up to the yield stress and macromolecular rearrangement. It may be influenced by intrinsic factors like the molecular structure, the cohesion energy, the molecular weight and the morphology. The morphological aspect is frequently one of the most important factors. On the other hand, strain hardening is also strongly influenced by extrinsic factors such as the temperature, the stress amplitude and the strain rate [27]. For confined cyclic loading like that imposed to fiber-matrix interface zones during fatigue loading, strain hardening may highly increase [28]. The result is a local rise in the yield and failure stresses or the strain of the interface-interphase, which leads to an apparent growth of the fiber-matrix strength.

Moreover, the experimental results shown previously emphasize a diffusive nature of the local damage in SMC composites. In other words, when an interface breaks, the local stress is systematically redistributed on other undamaged locations. Consequently, the average interfacial stresses of the undamaged fibers progressively increase during fatigue damage, which goes with an amplification of interface-interphase material strain hardening.

Therefore, in order to take into account the local effect of cyclic loading on the fiber-matrix interface apparent resistance, we may consider that the associated local failure criterion requires a progressive increase in the interfacial strength parameters σ_0 and τ_0. This evolution should be relative to:

(a) The local interfacial stress amplitudes σ and τ
(b) The number of applied cycles N

4.2. Fatigue damage prediction procedure

Since the evolution of the interfacial strength parameters are identified, we may use the micromechanical damage model presented above to predict fatigue damage. To this end, we propose an algorithm shown in Fig. 9: The input data include the elastic characteristics of the

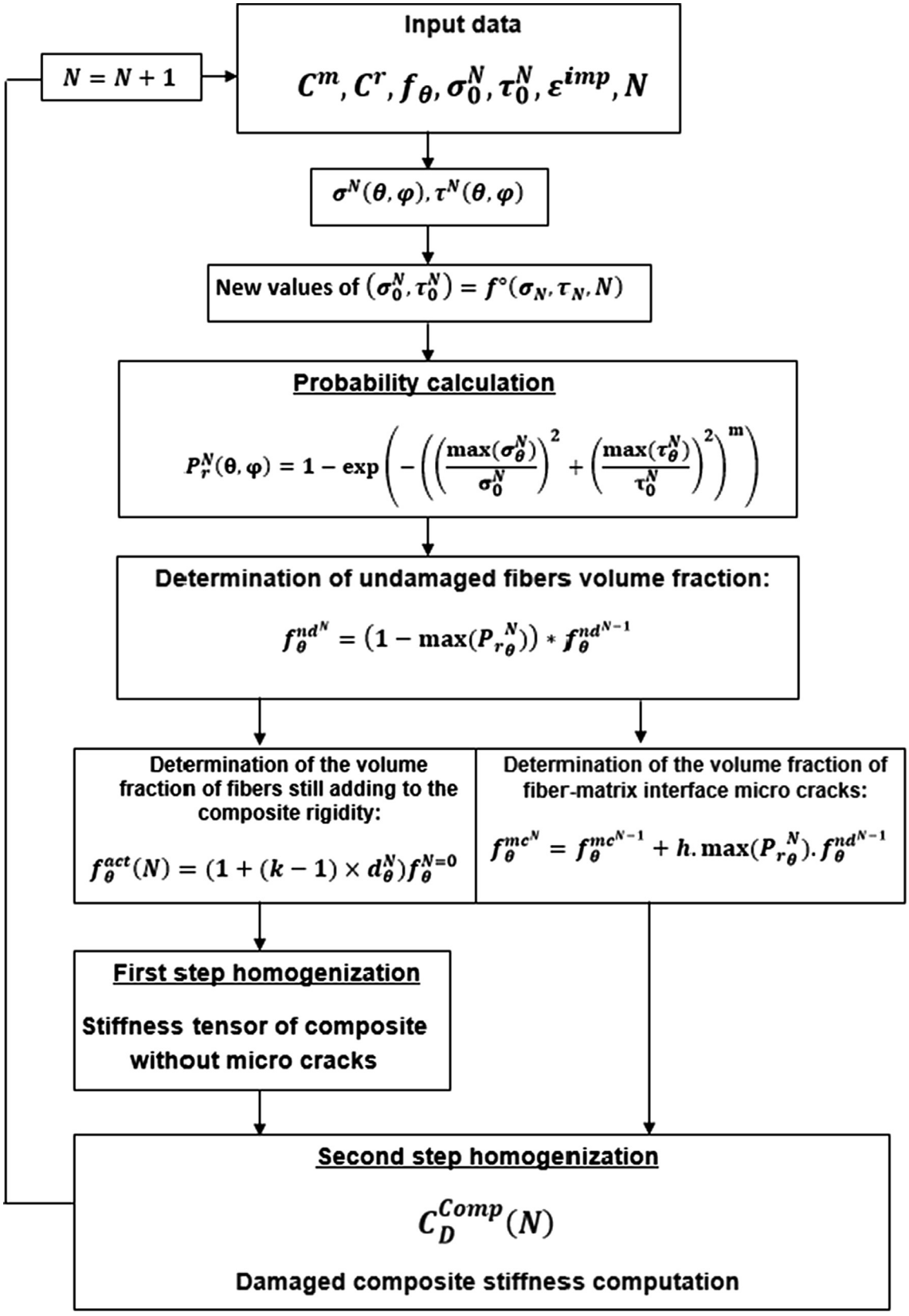

Fig. 9. Micromechanical fatigue damage prediction algorithm.

different phases, the fiber orientation distribution (Fig. 3), the initial interfacial strength parameters σ_0 and τ_0 (identified in Section 3.3), the imposed macroscopic cyclic strain ε^{imp}, and the current number of imposed cycles N.

Interfacial stress fields $\sigma^N(\theta, \varphi)$, $\tau^N(\theta, \varphi)$may be calculated for each fiber-matrix interface location (θ, φ). Thus, the maximum value of the interfacial failure probability can be determined for each fiber orientation in order to compute the new corresponding volume fractions

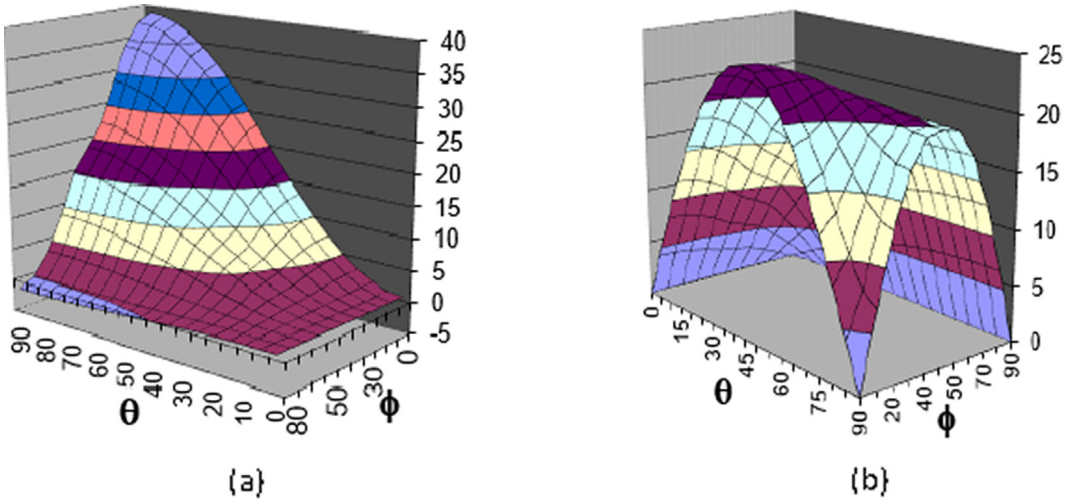

Fig. 10. Distribution of normal (a) and shear (b) stresses for 1 MPa magnitude tensile loading.

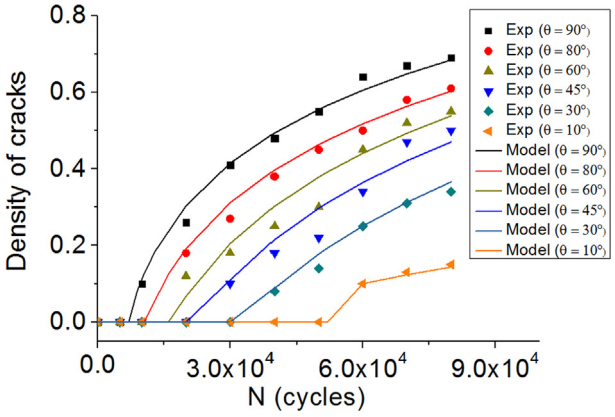

Fig. 11. Comparison between experimental and simulated density evolutions of fiber-matrix interface microcracks for several orientations.

of the fibers remaining undamaged. At the same time, the density distributions of active fibers (still contributing to the composite stiffness) and interfacial microcracks are computed. Hence, a first step homogenization, including active fibers only, is performed. Then, second-step homogenization allows determining the whole damaged composite, including active fibers and fiber-matrix interface micro-cracks for the considered number of cycles and the imposed macroscopic strain. After incrementation, a new value of the applied number of cycles is defined, and this procedure is repeated.

4.3. Fiber-matrix interface cyclic damage criterion identification

Based on the above algorithm, we propose to identify the evolutions of σ_0 and τ_0 as a function of σ, τ and N. Accordingly, we analyze the local interfacial stress state under tensile fatigue loading. Fig. 10 illustrates the evolution of the normal (Fig. 9a)) and shear (Fig. 9b)) stresses computed using the Mori and Tanaka model for a tensile stress of 1 MPa magnitude applied to the SMC composite in study. It can be easily observed that the maximum values of the normal and shear stresses are observed for $\theta = 90^{\circ}$, $\varphi = 0^{\circ}$ and $\theta = 45^{\circ}$, $\varphi = 0^{\circ}$, respectively.

Thus, we suggest a two-step identification procedure using the reverse engineering method based on the above algorithm and the density evolutions of the interfacial cracks determined experimentally for $\theta = 90^{\circ}$ and $\theta = 45^{\circ}$ populations of fibers.

The first step is assigned to the identification of the evolution of σ_0 on the basis of the density evolution of the interfacial cracks determined experimentally for the most disoriented fibers ($\theta = 90^{\circ}$). Indeed, in accordance with the stress fields of Fig. 10, tensile damage always begins in this location. Moreover, the interface damage of 90° oriented fibers is the most intensive: Near final failure, more than 80° of these fibers show broken interfaces. It is noted that debonding is always observed at the interfacial point defined by $\varphi = 0^{\circ}$ (see Fig. 4a)). At this point, $\tau = 0$.

Therefore, for a given fiber orientation, the corresponding fiber-matrix interface failure probability is given by:

$$\Pr_{\theta}^{N} = 1 - \exp\left[-\left(\left(\frac{\sigma^{N}}{\sigma_{0}^{N}}\right)^{2m}\right)\right] \tag{10}$$

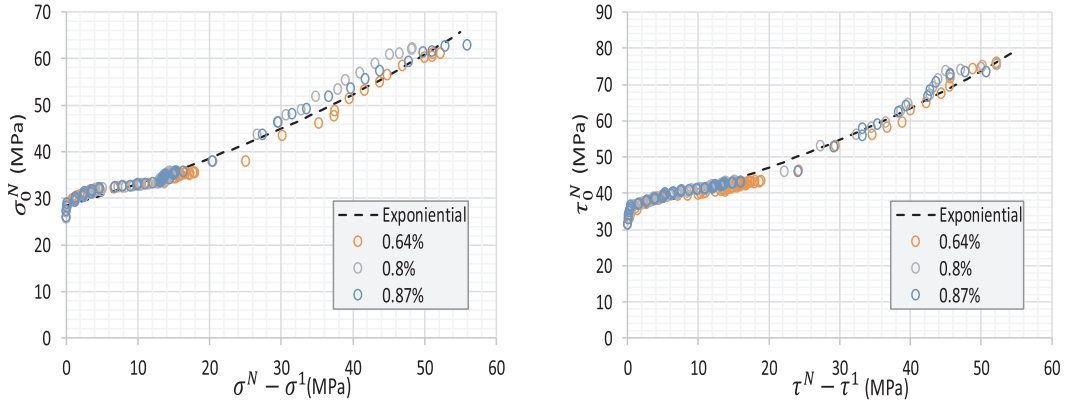

Fig. 12. Evolutions for three values of the macroscopic applied strains: 0.64%, 0.8% and 0.87% for θ = 0° and θ = 45°.

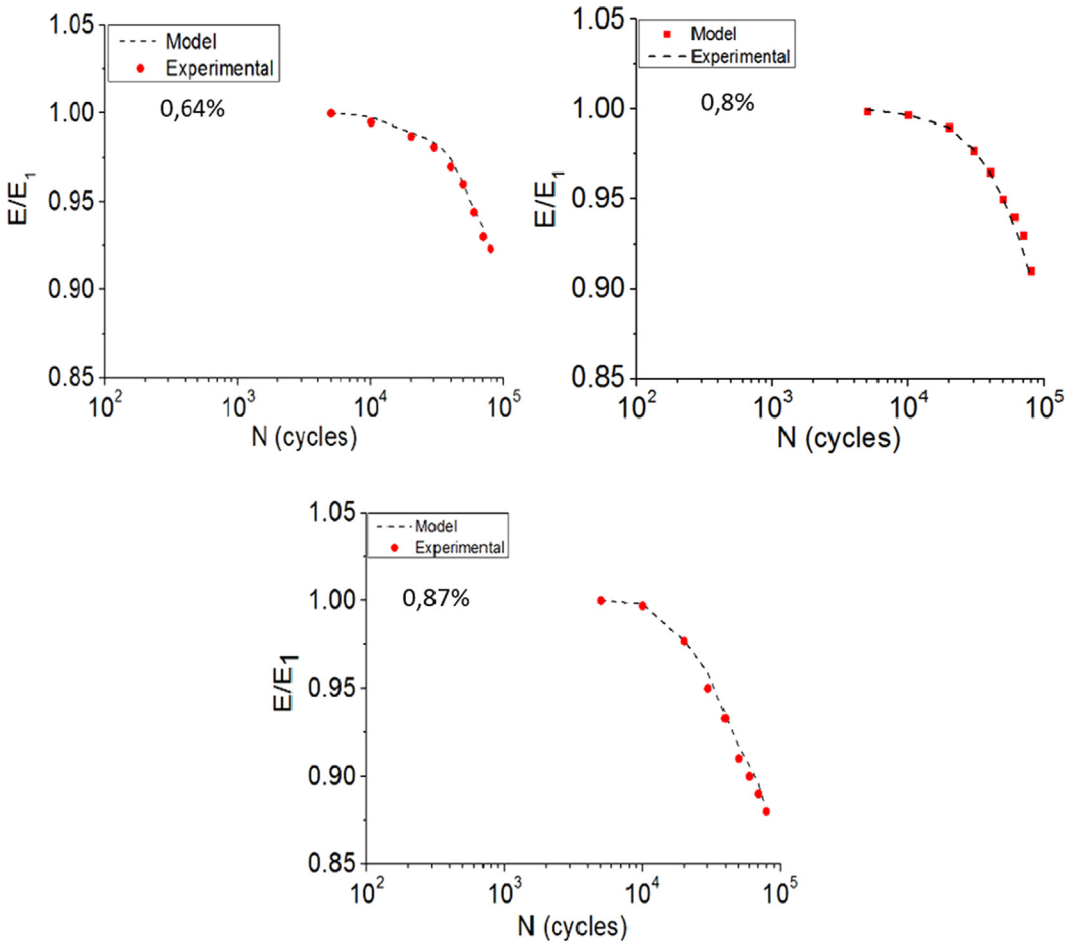

Fig. 13. Comparison of model and experimental curve for evaluation of relative modulus per number of cycles for SMC, imposed amplitude: 0.64%, 0.8% and 0.87%.

Furthermore, each N increment corresponds to a local damage increase:

$$\Delta d_{90^\circ}^{N} = d_{90^\circ}^{N} - d_{90^\circ}^{N-1}.$$

Then, the fiber-matrix interface failure probability can be also written as

$$Pr_{90^\circ}^{N}(N) = \frac{d_{90^\circ}^{N} - d_{90^\circ}^{N-1}}{1 - d_{90^\circ}^{N-1}} \tag{11}$$

Moreover, from Eq. (2), the probability can be rewritten as:

$$Pr_{90^\circ}^{N}(N) = \frac{A_{90^\circ} * \ln(\frac{N}{N-1})}{1 - A_{90^\circ} * \ln(N-1) + B_{90^\circ}} \tag{12}$$

Finally, the evolution of σ_0 is derived from Eqs. (13) and (15) as follows:

$$\sigma_0^N = \frac{\sigma^N}{[-Ln(T_{90^\circ}^{N})]^{(\frac{1}{2m})}} \tag{13}$$

$$\text{with} T_{90^\circ}^{N} = 1 - \frac{A_{90^\circ} * \ln(\frac{N}{N-1})}{1 - A_{90^\circ} * \ln(N-1) + B_{90^\circ}} \tag{14}$$

Once the evolution of σ_0^N is identified, we may consider the evolution of the shear stress threshold τ_0 during fatigue loading. To this aim, the experimental interfacial damage evolution of fibers oriented at 45° should be considered in reverse engineering identification. Indeed, it may be observed that for this fiber orientation, each interfacial location is submitted to both normal and shear stresses. Furthermore, since the maximum shear is observed on the 45° oriented fiber interfaces, the local cyclic effect discussed in Section 4.1 should be maximal for this orientation. Like the σ_0^Nidentification, the τ_0^N evolution can be derived from Eq. (2), Eq. (9) and Eq. (14) applied to the 45° oriented fibers:

$$\tau_0^N = \frac{\tau^N}{\left[[-\ln(T_{45^\circ}^{N})]^{(\frac{1}{m})} - \left(\frac{\sigma^N}{\sigma_0^N}\right)^2\right]^{\frac{1}{2}}} \tag{15}$$

$$\text{with} \quad T_{45^\circ}^{N} = 1 - \frac{A_{45^\circ} * \ln(\frac{N}{N-1})}{1 - A_{45^\circ} * \ln(N-1) + B_{45^\circ}} \tag{16}$$

Finally, identified σ_0^N and τ_0^N should be validated by comparing between the density evolutions of predicted and experimental fiber-matrix microcracks during fatigue for other orientations (namely 10°, 30°, 65° and 80°). The good correlation depicted in Fig. 11 validates our approach.

4.4. Stiffness reduction prediction

4.4.1. Local criterion analysis

The main idea of our approach is to reflect fiber-matrix interface strain hardening during cyclic loading. Because this phenomenon arises at a local scale, this evolution should be independent of imposed macroscopic loading. Indeed, Eqs. (16)–(19) clearly convey that the interfacial strength evolution is related to local interfacial stresses (σ^N and τ^N) which increase together with the applied number of cycles. Since the local interfacial stress undergone at the first cycle depends on the macroscopic applied strain, it is judicious to plot the evolution of identified σ_0^N and τ_0^N during fatigue as a function of $\sigma^N - \sigma^1$ and

$\tau^N - \tau^1$, where σ^1 and τ^1 are the first cycle fiber-matrix normal and shear stresses, respectively.

Fig. 12 shows these evolutions for three values of the macroscopic applied strain: 0.64%, 0.8% and 0.87% for $\theta = 0^\circ$ and $\theta = 45^\circ$.

Therefore, as a first approximation, one may propose a mathematical form to the evolutions of fiber-matrix interface failure criterion parameters during fatigue:

$$\sigma_0^N = a * \exp((\sigma^N - \sigma^1)^b)$$

$$\tau_0^N = c * \exp((\sigma^N - \sigma^1)^d)$$

where *a, b, c* and *d* are material parameters to be identified.

4.4.2. Stiffness reduction prediction

Fatigue tests performed at several values of the imposed macroscopic strain allow plotting the evolution of the stiffness reduction during cyclic loading. Fig. 13 illustrates the comparison between simulated stiffness reduction and experimental stiffness decrease for the three imposed strain levels (0.64%, 0.8% and 0.87%).The predicted Young's modulus reduction agrees well with the experimental observations.

5. Conclusion

The dominant damage mechanism of SMC materials is interfacial decohesion. Under fatigue loading, it leads to the degradation of the mechanical properties, i.e. progressive reduction in stiffness. A formulation of a micromechanical damage constitutive model is presented to predict stiffness reduction as a function of the number of fatigue cycles and the local stress state. This model is based on a quadratic interfacial criterion expressed in terms of normal and shear local stresses at the fiber-matrix interface associated to their corresponding failure values. In order to reflect the effect of repeated loading at a fiber-matrix interface scale, the local normal and shear failure stresses should progressively increase in order to take into account the coupled effect of the local stress redistribution caused by damage and strain hardening of polymers located at the interface zone.

Therefore, this work principally aims to identify the mathematical form of the evolution of the proposed fiber-matrix interface failure criterion parameters during fatigue. To this end, an original inverse engineering methodology is proposed based on an accurate and complete experimental description of the interfacial damage, coupled to a micromechanical predictive damage model adapted to cyclic loading. It is shown that the identified local fatigue damage criterion can be simply represented by an exponential increasing shape as a function of the gap between the current local stresses (i.e. for the considered number of cycles) and the local stresses undergone during the first applied cycle. This expression should be considered as a representative of the fiber-matrix strain hardening fatigue effect in short fiber reinforced composites. Thus, the identification of the criterion should be based on a simple reverse engineering using only macroscopic stiffness reduction during tensile fatigue. Hence, there is no more need to perform a complete local damage experimental analysis.

Moreover, it should be mentioned that this criterion is independent of the macroscopic tridimensional applied loading, as a consequence of its local nature. Therefore, it may be identified on the basis of simple tensile cyclic loading results and be applied to a real structure design for anisotropic stiffness reduction prediction.

At the end of the paper, the proposed approach is validated through a comparison between experimental and simulated losses of stiffness for several values of a maximal imposed strain.

Declaration of Competing Interest

The authors declare that they have no known competing financial interests or personal relationships that could have appeared to influence the work reported in this paper.

References

[1] Feuillade A, Bergeret V, Quantin A, Crespy J. Characterisation of glass fibres used in automotive industry for SMC body panels. Compos. Part A Appl. Sci. Manuf. 2006;37(10):1536–44.

[2] Shirinbayan M, Fitoussi J, Abbasnezhad N, Meraghni F, Surowiec B, Tcharkhtchi A. Mechanical characterization of a Low Density Sheet Molding Compound (LD-SMC): Multi-scale damage analysis and strain rate effect. Compos B Eng 2017;131:8–20. https://doi.org/10.1016/j.compositesb:2017.08.004.

[3] Oldenbo M, Fernberg SP, Berglund LA. Mechanical behaviour of SMC composites with toughening and low density additives. Compos. Part A Appl. Sci. Manuf. 2003;34(9):875–85.

[4] Palmer J, Savage L, Ghita OR, Evans KE. Sheet moulding compound (SMC) from carbon fibre recyclate. Compos. Part A: Appl. Sci. Manuf. 2010;41(9):1232–7.

[5] Fotouh A, Wolodko JD, Lipsett MG. Fatigue of natural fiber thermoplastic composites. Compos. PART B 2014;62:175–82.

[6] Chaturvedi SK, Sun CT, Sierakowski RL. Mechanical characterization of sheet molding compound composites. Polym. Compos. 1983;4(3):167–71.

[7] Naebe M, Abolhasani MM, Khayyam H, Amini A, Fox B. Crack damage in polymers and composites: A review. Polym. Rev. 2016;56(1):31–69.

[8] Van Paepegem W. Fatigue damage modelling of composite materials with the phenomenological residual stiffness approach. Fatigue Life Prediction of Composites and Composite Structures. Elsevier; 2010. p. 102–38.

[9] Mughrabi H. Assessment of fatigue damage on the basis of nonlinear compliance effects. Handbook of Materials Behavior Models. Elsevier; 2001. p. 622–32.

[10] Socie DF, Marquis GB. Multiaxial fatigue. Compr. Struct. Integr. Cycl. Load. fatigue 2003;4:221–52.

[11] Quaresimin M, Ricotta M. 9 - Fatigue response and damage evolution in 2D textile composites BT - Fatigue of Textile Composites. Woodhead Publishing Series in Composites Science and Engineering. Woodhead Publishing; 2015. p. 193–221.

[12] Plumtree A, Cain K. Fatigue damage accumulation in CFRP. High Perform. Struct. Mater. IV 2008;I:275–83.

[13] Capela C, Costa JD, Ferreira JAM. Test conditions effect on the fracture toughness of hollow glass micro-sphere filled composites. Strain 2008;44(2):141–6.

[14] Jendli Z, Fitoussi J, Meraghni F, Baptiste D. Anisotropic strain rate effects on the fibre-matrix interface decohesion in sheet moulding compound composites. Compos. Sci. Technol. 2005;65(3–4):387–93.

[15] Jendli Z, Meraghni F, Fitoussi J, Baptiste D. Micromechanical analysis of strain rate effect on damage evolution in sheet molding compound composites. Compos. Part A Appl. Sci. Manuf. 2004;35(7–8):779–85.

[16] Tamboura S, Sidhom H, Baptiste D, Fitoussi J. Evaluation de la tenue en fatigue du composite SMC R42. Matér. Tech. 2001;89(3-4):3–11http://www.mattech-journal.org/10.1051/mattech/200189030003https://doi.org/10.1051/mattech/200189030003.

[17] Laribi MA, Tamboura S, Fitoussi J, Tié Bi R, Tcharkhtchi A, Ben Dali H. Fast fatigue life prediction of short fiber reinforced composites using a new hybrid damage approach: application to SMC. Compos B Eng 2018;139:155–62https://linkinghub.elsevier.com/retrieve/pii/S1359836817320346https://doi.org/10.1016/j.compositesb:2017.11.063.

[18] Fitoussi J, Meraghni F, Jendli Z, Hug G, Baptiste D. Experimental methodology for high strain-rates tensile behaviour analysis of polymer matrix composites. Compos Sci Technol 2005;65:2174–88.

[19] Shirinbayan M, Fitoussi J, Meraghni F, Farzaneh S, Surowiec B, Tcharkhtchi A. Effect of a post-fatigue damage on the residual dynamic behavior of advanced-SMC composites. Appl. Compos. Mater. 2019:1–19.

[20] Shirinbayan M, Fitoussi J, Meraghni F, Laribi M, Surowiec B, Tcharkhtchi A. Coupled effect of loading frequency and amplitude on the fatigue behavior of Advanced Sheet Molding Compound (A-SMC). J. Reinf. Plast. Compos. 2017;36(4):271–82.

[21] Shirinbayan M, Fitoussi J, Bocquet M, Meraghni F, Surowiec B, Tcharkhtchi A. Multi-scale experimental investigation of the viscous nature of damage in Advanced Sheet Molding Compound (A-SMC) submitted to high strain rates. Compos. B Eng. 2017;115:3–17.

[22] Shirinbayan M, Fitoussi J, Meraghni F, Surowiec B, Bocquet M, Tcharkhtchi A. High strain rate visco-damageable behavior of Advanced Sheet Molding Compound (A-SMC) under tension. Compos. B Eng. 2015;82:30–41.

[23] Jendli Z, Meraghni F, Fitoussi J, Baptiste D. Multi-scales modeling of dynamic behaviour for discontinuous fibre SMC composites. Compos. Sci. Technol. 2009;69:97–103.

[24] Baptiste D. Damage micromechanics modelling of discontinuous reinforced composites. Continuum Damage Mechanics of Materials and Structures. Elsevier Science Ltd; 2002.

[25] Fitoussi J, Guo G, Baptiste D. A statistical micromechanical model of anisotropic damage for smc composites. Compos. Sci. Technol. 1998;58(5):759–63.

[26] Ayari H, Fitoussi J, Imaddahen A, Tamboura S, Shirinbayan M, Ben Dali H, et al. Two hybrid approaches to fatigue modeling of Advanced-Sheet Molding Compounds (A-SMC) composite. Appl Compos Mater 2020.

[27] Robert SHOY, Robbins Mark O. Strain hardening of polymer glasses: effect of entanglement, density, temperature, and rate. J. Polym. Sci. Part B: Polym. Phys. 2006;44:3487–500.

[28] Jain A, Van Paepegem W, Verpoest I, Lomov SVSV. A statistical treatment of the loss of stiffness during cyclic loading for short fiber reinforced injection molded composites. Compos. Part B 2016;103:40–50. https://doi.org/10.1016/j.compositesb.2016.08.002.